Sulfur-containing particles emitted by concealed sulfide ore deposits: An unknown source of sulfur-containing particles in the atmosphere

Jianjin Cao[a,b]*, Yingkui Li[a], Tao Jiang[a], Guai Hu[a]

a School of Earth Science and Geological Engineering, Sun Yat-sen University, Guangzhou, People's Republic of China 510275

b Guangdong Key Laboratory of Geological Process and Mineral Resources Exploration, Guangzhou, Guangdong 510275, P.R. China

Abstract

Sources of sulfur dioxide, sulfates, and organic sulfur compounds, such as fossil fuels, volcanic eruptions, and animal feeding operations, have attracted considerable attention. In this study, we collected particles carried by geogas flows ascending through soil, geogas flows above the soil that had passed through the soil, and geogas flows ascending through deep faults of concealed sulfide ore deposits and analyzed them using transmission electron microscopy. Numerous crystalline and amorphous sulfur-containing particles or particle aggregations were found in the ascending geogas flows. In addition to S, the particles contained O, Ca, K, Mg, Fe, Na, Pb, Hg, Cu, Zn, As, Ti, Sr, Ba, Si, etc. Such particles are usually a few to several hundred nanometers in diameter with either regular or irregular morphology. The sulfur-containing particles originated from deep-seated weathering or faulting products of concealed sulfide ore deposits. The particles suspended in the ascending

geogas flow migrated through faults from deep-seated sources to the atmosphere. This is a previously unknown source of the atmospheric particles. This paper reports, for the first time, the emission of sulfur-containing particles into the atmosphere from concealed sulfide ore deposits. The climatic and ecological influences of these sulfur-containing particles and particle aggregations should be assessed.

Keywords: sulfur-containing particles, ascending gas flow, unknown source, sulfide ore deposits.

*Corresponding author. Tel.: 862084035033; Fax: 862084035033

E-mail address: eescjj@mail.sysu.edu.cn

1. Introduction

Sources of sulfur oxides, sulfates, and organic sulfur compounds are diverse and associated with natural and anthropogenic activities. Known sources of sulfur are volatile sulfur compounds derived from animal feeding operations (Trabue et al., 2008), and aerobic decomposition of food waste (Wu et al., 2010), biogenic sulfur from rice paddies (Yang et al., 1996; Yang et al., 1998) and the Subantarctic and Antarctic Oceans (Berresheim, 1987), sulfur gas (H_2S and SO_2) from geothermal fields (Kristmannsdottir et al., 2000), organic sulfur compounds from sediments and immature crude oil (Sinninghe Damsté et al., 1988), sulfur oxides from the oxidation of fossil fuels (Soleimani et al., 2007), and sulfur dioxide from acid factories and volcanic eruptions (Wong 1978; Sweeney et al., 2008). Sulfate particles, which are important anthropogenic aerosols and influencing climate (Pósfai et al., 1997; Williams et al., 2001), occur in mineral dust (Kiehl, 1999). Furthermore, volcanic activity is a major contributor of sulfur to the atmosphere (Zreda-Gostynska et al., 1993; Graf et al., 1998; Streets et al., 2000; Seino et al., 2004; Bhugwant et al., 2009; Bao et al., 2010; Gierén and Querol, 2010), particularly in countries such as Japan, Indonesia, Réunion Island, the Philippines, Iceland, Guatemala, and New Zealand (Rose et al., 1986; Andres et al., 1993; Streets et al., 2000; Seino et al., 2004; Chenet et al., 2005; Bhugwant et al., 2009).

Stratospheric sulfur adds very little to the environmental consequences of the anthropogenic sulfur that is released in the troposphere and deposits within days to weeks (Wong, 1978; Chenet et al., 2005). Existing research shows that SO_2 is

55 oxidized to SO_4^{2-} in both the gas and liquid phases. Moreover, sulfate aerosols can
56 directly affect the climate (Graf et al., 1998). In our previous work, particles carried
57 by an ascending geogas flow in the soil (Holub et al., 1999; Cao et al., 2009, 2010b;
58 Cao et al., 2011; Liu et al., 2011; Wei et al., 2013) were studied and found to contain
59 sulfur. Further research showed that sulfur-containing particles carried by ascending
60 geogas flows can be transported through the soil layers and into the atmosphere.
61 Sulfur-containing particles suspended in the ascending geogas flow migrate through
62 faults from deep-seated concealed sulfide ore deposits to the Earth's surface. These
63 particles are a previously unknown source of sulfur-containing particles in the
64 atmosphere. This paper reports, for the first time, the emission of sulfur-containing
65 particles into the atmosphere from concealed sulfide ore deposits. Because concealed
66 sulfide ore deposits are widely distributed, the influence of sulfur-containing particles
67 derived from them is important. The climatic and ecological effects of these particles
68 should be studied.

69 2. Methods

70 Particles carried by an ascending geogas flow above the soil (that had flown through
71 the soil), in the soil, and in deep-seated faults were collected at the Dongshengmiao
72 polymetallic sulfide deposit in the Inner Mongolia Autonomous Region, China.
73 Particles carried by the ascending gas flow in the soil were also collected at other
74 concealed ore deposits containing sulfide minerals, such as the Kafang copper deposit
75 of the southern Yunnan Province, the Yongshengde copper deposit in northeastern

Yunnan, and the Qingmingshan copper–nickel sulfide deposit in Guangxi Province, China.

Particles transported by the ascending geogas flow above the soil (that had flown through the soil) were sampled using stainless steel tubes and carbon-coated nickel transmission electron microscopy (TEM) grids. The length of the stainless steel tubes was 40 cm and their diameter was 2.8 cm. These tubes were inserted vertically into the soil to a depth of about 30 cm. A carbon-coated nickel TEM grid was fixed at the end of the stainless steel tubes. The ascending geogas flow in the soil moved into the stainless steel tubes and naturally passed through the 30 cm soil layer. Then, the gas flow passed through the 10 cm of the empty stainless steel tubes above the soil. Finally, the geogas flow arrived at the top of the tubes. Particles carried by the geogas flow were adsorbed onto the carbon-coated nickel TEM grid. A protective device was installed on the outside of the steel tubes to ensure that particles sampled were those carried by the ascending geogas flow. The protective device is a cylindrical polyethyleneterephthalate bottle. A small hole at the side of the bottle allowed the outflow of ascending geogas flow; however, adsorption material placed in the hole did not allow the external particles to enter. Sampling devices were installed between July 25, and August 23, 2013, and the carbon-coated nickel TEM grids were retrieved on September 8, 2013. Sampling sites were distributed across a fault above the concealed sulfide ore bodies of the Dongshengmiao polymetallic sulfide deposit.

Particles transported by the ascending geogas flow in the soil were collected using ordinary plastic funnels. An inverted funnel was inserted in a hole that was 60–80 cm

deep and backfilled with soil, and a TEM grid was fixed at the end of the funnel spout with nylon net. The setup was protected from contamination using plastic pipes and cups. The TEM grids were retrieved after 60 days.

Particles carried by ascending geogas flows in deep-seated faults were sampled using two methods. The first method used an active sampling device with a vacuum pump, polyvinyl chloride (PVC) pipe and carbon-coated nickel TEM grid as the main components. One end of the PVC pipe was connected with a tubing to the pump. A drilling steel was inserted slantwise into the fault. The inserted depth was 30–50 cm. As the drilling steel was pulled out, the PVC pipe was inserted into the hole. The PVC pipe was compacted using fault gouge. The impurity gases in the PVC pipe were pumped out using the vacuum pump, then, the PVC pipe was quickly sealed. A day later, we connected a tube equipped with a carbon-coated nickel TEM grid to the PVC pipe. The gas was pumped using a vacuum pump and flowed through the TEM grid for 1 to 2 hours. Particles carried by the gas were collected by the TEM grid. Finally, the carbon-coated nickel TEM grid was removed and sealed in a sample cell. The second method did not use a vacuum pump. A carbon-coated nickel TEM grid was fixed to the end of the PVC pipe. The ascending geogas flow in the fault flowed into the PVC pipe and arrived at the top of the PVC pipe naturally. The particles carried by the geogas flows in the faults were adsorbed onto the carbon-coated nickel grid. The sampling devices were installed on August 3–10, 2013, and the TEM grids were retrieved on September 7, 2013.

High-resolution TEM analyses were performed using a Tecnai G2 F30 S-TWIN

instrument at Yangzhou University, China, using an accelerating voltage of 300 kV. The grids were checked using TEM before sampling to ensure they were devoid of particles.

3. Results

3.1 Sulfur-containing particles carried by an ascending geogas flow above the soil (that had flown through the soil)

According to the TEM analysis, particles containing high levels of S, O, Pb, Zn, Fe, Hg, As, etc, were found in the ascending gas flows above the soil above the Dongshengmiao polymetallic sulfide deposit. Table 1 provides the number of sulfur-containing particles or particle aggregations that were found on the 100 μm × 100 μm TEM grid. In general, one aggregation included more than five particles. Figure 1 shows an elliptical particle (ID: 1) having a diameter of 500 nm. The particle contains 78.17% S and 18.47% O (Table 2). Its O to S atomic ratio is 0.47. Figure 2 shows a particle aggregation (ID: 2) that consists of several small particles having a diameter of 3–8 nm. It contains 31.23% S and 59.29% Hg. The spacing of the lattice fringes was measured to be 0.333 nm. Figure 3 shows particle aggregations (ID: 3) with sizes of less than 100 nm. Their O to S atomic ratio is 0.51. The particle aggregations contain 14.48% Pb. The particle (ID: 4) illustrated in Figure 4 is elliptical with a diameter of 200 nm and contains 18.55% As, 54.2% Pb, and 8.34% Zn. The particle (ID: 5) shown in Figure 5 contains 2.25% Co. It is amorphous and has an O to S atomic ratio of 2.91. The particle aggregation (ID: 6) illustrated in Figure 6 contains 62.39% Cu and consists of small particles each having a diameter of

142 5–10 nm. Figure 7 presents a particle aggregation (ID: 7) that consists of many small
143 particles with diameters of about 5 nm, and contains 69.28% Pb.
144 3.2 Sulfur-containing particles carried by an ascending gas flow in the soil
145 Numerous sulfur-containing particles transported by an ascending gas flow were
146 found in the soil over sulfide ore deposits. Figure 8 shows an aggregation of such
147 particles from the Dongshengmiao polymetallic sulfide deposit. The aggregation (ID:
148 8) may be composed of $CaSO_4$ with trace amounts of K, Mg, Fe, and Si. It is regularly
149 shaped and 300 nm in size. The selected area electron diffraction pattern shows that
150 the aggregation is polycrystalline, possibly gypsum. Figure 9 shows a TEM image of
151 a sulfur-containing particle (ID: 9) from the Kafang copper deposit, South China.
152 Sulfur accounts for 63.99% of the particle (Table 3), and its O to S atomic ratio is 0.83.
153 Its K content is 8.93%, and its size is 330 nm. Figure 10 shows a regularly polygonal
154 particle (ID: 10) from the Yongshengde copper deposit, China. Its O to S atomic ratio
155 is 3.60, and its Fe and F contents are 9.94% and 1.71%, respectively. Figure 11 shows
156 a sulfur-containing particle (ID: 11) from the Qingmingshan Cu–Ni sulfide deposit,
157 Guangxi Province, China. Its O to S atomic ratio is 2.51. The particle contains 2.03%
158 Co and is 300 nm × 400 nm in size. The selected area electron diffraction pattern
159 shows that the particle is amorphous.
160 3.3 Sulfur-containing particles carried by ascending geogas flows in deep-seated
161 faults
162 Sulfur-containing particles were found in samples obtained using two methods from
163 the deep fault gas of the Dongshengmiao polymetallic sulfide deposit. Figure 12

shows a sulfur-containing particle aggregation (ID: 12) that was obtained using the vacuum pump from the deep-seated fault gas near a concealed ore body. The aggregation contains O, Na, Si, S, K, Fe, Zn, and Pb. The S content is 23.8%. Figure 13 shows a particle aggregation (ID: 13) that was obtaied using a PVC pipe from a fault near a concealed ore body. The ascending gas flow arrived at the top of the PVC pipe naturally, and the particles were adsorbed by a TEM nickel grid. The particle aggregation consists of many small particles that are 4–15 nm in diameter. The small particles are elliptical and crystalline, with 0.302 nm spacing of the lattice fringes, and and their main components are O and S. Figure 14 shows a sulfur-containing particle (ID: 14) that was sampled using a PVC pipe in a fault above a concealed ore body. The vertical distance from the sample to the concealed ore body was 85 m. The vertical distance from the sample to the Earth's surface was 230 m.

3.4 Sulfur-containing particles in deep-seated fault gouges and oxidized ores

Sulfur-containing particles were also found in deep-seated fault gouges and oxidized zones of the Dongshengmiao polymetallic sulfide deposit. For example, Figure 15 shows a sulfur-containing particle (ID: 15) from the oxidized zone. According to its atomic percentage，it contains SO_4^{2-} and may be Sr, Ba sulfate, and Ti oxide. Its size is 200 nm × 400 nm. Figure 16 shows a rhombus-shaped particle (ID: 16) from a deep-seated fault gouge. Its main components are O, S, and Ca, with minor amounts of Fe, Co, and Si.

Overall, the sulfur-containing particles or particle aggregations transported by ascending geogas flows can be both regular and irregular in shape and either

crystalline or amorphous. The particles or particle aggregations contain Ca, K, Mg, Fe, Na, Pb, Hg, Cu, Zn, As, Ti, Sr, Ba, and Si, as well as O and S.

The number of sulfur-containing particles in the ascending geogas flows in non-sulfur-rich areas is much lower than that from the sulfide ore deposits. Furthermore, the overwhelming majority of particles in non-sulfur-rich areas have a low sulphur content. These areas are different from those with the sulfide ore deposits, in which sulfur-containing particles are densely distributed and are present at high levels in the ascending geogas flows.

4. Discussion and conclusions

Gold particles are formed by post-mineralization fault activity, oxidation, and bacterial weathering of primary minerals (Cao et al., 2010a). Deep-seated gold particles can be transported to the surface by an ascending gas flow, as Brownian motion enables the gold particles in the ascending gas flow to overcome the effect of gravity (Cao et al., 2010a; Cao, 2011). We assume that the same mechanism applies to sulfur-containing particles or particle aggregations. Primary sulfur-containing minerals are transformed into particles by epigenetic reworking, such as post-mineralization fault activity, in which S^{2-} in the sulfide minerals is oxidized to S^{6+}. In this study, the sulfur-containing particles from fault gouges and oxidized ores were found, indicating that these particles were formed by the faulting and oxidation of ores. Faulting and oxidation are well-developed in the Dongshengmiao polymetallic sulfide deposit and other sulfide deposits. This finding indicates that faulting and oxidation play an important role in particle formation.

Sulfur-containing particles may be transported to the surface by an ascending geogas flow through faults. Because gases and particles move along faults, they can migrate over long distances (Etiope and Martinelli, 2002; Cao et al., 2010a). Material carried by an ascending geogas flow in the soil in the Xuanhan gas field, Sichuan Province, China was sampled and measured using an instrumental neutron activation analysis. Analysis of trace element anomalies has shown the gas-bearing ring fracture structure to be 4000 m deep, suggesting that particles carried by an ascending geogas flow can be transported over long distances (Yang et al., 2000). The gas flow migrates upward because of the temperature difference and the pressure differences between the Earth's interior and its surface is the reason that the gas flow migrate upward (Tong and Li, 1999; Etiope and Martinelli, 2002; Cao et al., 2010a). In this study, the particles or particle aggregations were found in ascending geogas flows in faults at different depths near or above the concealed ore bodies of the Dongshengmiao polymetallic sulfide deposit. This observation demonstrates that the faults are channels for particles carried by the ascending geogas flow. Sulfide-containing particles suspended in gas above the soil were found, showing that these particles can move through the soil and get into the atmosphere.

The probability that these particles are transported by an ascending geogas flow originating in the soil is low. In the study area, the soil consists of kaolinite, halloysite, montmorillonite, illite, chlorite, hematite, quartz, goethite, and similar minerals. Kaolinite is the main mineral, and the sulfur content in the soil is low. Therefore, this soil is clearly not a probable source of sulfur-containing particles transported by an

ascending geogas flow. Furthermore, there is no correlation between the numbers of these particles and those of sulfur-containing particles in the soil solid phase. Sulfur-containing particles are clearly enriched in soils above deep sulfur-rich sources because sulfur-containing particles transported by an ascending geogas flow were found in 16 deep sulfide ore bodies that were studied. This result indicates a close relationship between sulfur-containing particles in the gas flow and deep-seated sulfide ore bodies. Other rock types, such as limestone, siltstone, sandstone, and mudstone, do not contain sufficient sulfur to become sources of sulfur-containing particles in an ascending gas flow; for example, the mean sulfur concentrations of the Devonian limestone, mudstone, siltstome, and sandstone in the northern Guangdong Province, China are 610×10^{-6} (68 samples), 80×10^{-6} (25 samples), 160×10^{-6} (33 samples), and 110×10^{-6} sulfur (4 samples), respectively.

For 16 ore deposits, in which we have studied particles carried by ascending geogas, a large number of sulfur-containing and Pb- and As-containing particles were found. There are oxidative ore bodies in many concealed sulfide ore deposits. As sulfide minerals change into oxide minerals, sulfide was released from these minerals. There are some sulfide concentration data for ascending geogas. Yuan et al. (China University of Geosciences, Beijing, China, 2014) analyzed sulfide concentrations of ascending geogas in soil at the Sunit deposit (the Inner Mongolia Autonomous Region, China), using plasma mass spectrographic analysis. Their sampling method allowed the flow of geogas in the soil through liquid collector slowly using a pump. The particles carried by the ascending geogas flow were adsorbed in the liquid collector.

The volume of the geogas extracted per hole was 5 liters. The geogas extracted from 3 holes (15 liters) was combined to make one sample. The liquid collector was made with high purity nitric acid and Mini-Q ultra pure water. The liquid collector was placed in a 25 ml polyethylene bottle. The analysis results from 1054 samples showed that the average sulfur content of the liquid collector was 26.4571 μg ml^{-1}. The maximum value was 35.33 μg ml^{-1} and the minimum value was 16.89 μg ml^{-1}. A concentration of 26.4571 μg ml^{-1} in the liquid collector may be translated into 44.095 mg per cubic meter of geogas flow. We know that sulfur-containing substances carried by geogas flow may be not completely adsorbed in the liquid collector. Therefore, the average sulfur content of the ascending geogas flow may have been higher than 44.095 mg per cubic meter. We analyzed the sulfide concentration of ascending geogas in the soil at the Kangjiawan deposit in the Hunan Province, China. Our sampling method is similarly to the method used by Yuan et al. (2014). The main difference is that our liquid collector was made with high purity aqua regia and tri-distilled water. The volume of the liquid collector was 100 ml. The volume of the geogas extracted from a hole was 9 liters. Therefore, the volume of the geogas extracted from 3 holes was 27 liters. The sulfide concentration of the liquid collector was analyzed using the plasma spectrum method. We analyzed the samples along 3 sections (sample numbers were 31, 74, and 20). The results showed that the average sulfur contents of the 3 sections were 0.27, 1.40, and 32.81 μg ml^{-1} respectively (Tables 4–6), which may be translated into 1.00, 5.19, and 121.50 mg per cubic meter of geogas flow, respectively.

There is earth degassing phenomena in metallic and nonmetallic deposits. The giant gold deposits, such as the Porcupine gold deposit in Canada, the Witwatersrand gold deposit in South Africa, and the Muruntau gold deposit in Uzbekistan, exhibit upward vertical movement of hydrocarbon gas. The Witwatersrand gold deposit has significant upward gas flow. In one day, 36700 m^3 of hydrocarbon gases degas from underground gold mining vents and 5×10^8 m^3 of hydrocarbon gases degas from 3000m or deeper mines every year. The Azerbaijan oil and gas region is strongly degassed, with 4×10^8 m^3 of gases degassed every year (Du, 2009). The ascending gas flow rates were measured to be between 60×10^{-4} and $4\ cm^3\ min^{-1}\ m^{-2}$ horizontally projected borehole area at three different sites by Malmqvist & Kristiansson (1984). Carbon dioxide concentrations above sulfide mineralizations are often enhanced. Hidden sulfide mineralizations at a depth of 200 m have been located in quartzite in areas such as Brittany, and sulphide ores have been located in granite in Cornwall. Above mineralizations, carbon dioxide in the soil gas has been found to increase to 10% from the normal concentration of 1%. The carbon dioxide flow may be as large as $0.2\ l\ m^{-2}\ h^{-1}$ (Hermansson et al. 1991). The Dongshengmiao deposit lies in a seismically active zone. The Langshan Mountain-front fault, in which minor earthquake activity frequently takes place and where M=6 earthquakes have taken place three times in the twentieth century, passes through the deposit. The release of geogas in active tectonic areas is widespread and occurs at a significant level (Judd et al., 1997; Etiope, 1999; Mörner and Etiope, 2002). The CO_2 emission flux of the Siena Graben Faults (Italy), Siena G. Arbia Fault (Italy), Ustica Arso Fault (Italy), and

San Andreas Fault (California) were 0.83–1123, 12.4–74.4, 77.3, and 0.4–23 kg m^{-2} $year^{-1}$ respectively (Etiope, 1995; 1999; Mörner and Etiope, 2002; Lewicki and Brantley, 2000). These equate, respectively, to 0.02–26.94, 0.3–1.78, 1.85, and 0.01–0.55 cm^3 m^{-2} s^{-1} if CO_2 density is assumed to be 1.3401 kg m^{-3}. The area of the Dongshengmiao deposit is 4.65 km^2. The emission flux estimation of the Dongshengmiao deposit was 0.5 cm^3 m^{-2} s^{-1} according to the emission fluxes of the above-mentioned faults and deposits. Therefore, the estimated degassing rate for the Dongshengmiao deposit was 2.325 m^3 s^{-1}. The distribution areas of concealed sulfur ore deposits are different. The ore deposits with the distribution areas of 1–12 km^2 may have more deposits than other areas. Concealed metal deposits containing sulfide minerals can be very extensive, such as the Killik massive sulfide deposit in northeastern Turkey (Çiftçi et al., 2005), the Masa Valverde blind massive sulfide deposit in Spain (Ruiz et al., 2002), and the Huize carbonate-hosted Zn–Pb–(Ag) District in South China (Han et al., 2007). Concealed sulfur nonmetallic deposits, such as gypsum and barite, are also widely distributed. The number of concealed sulfide deposits is far greater than those of active volcanoes. Under the climate-warming conditions, oxidation of sulfur-containing minerals is particularly accelerated.

Such sulfur-containing particles enter the atmosphere. Several studies have discussed the direct effects of sulfate particles on the climate (Liu et al., 2009). Some researchers have suggested that sulfur-containing particles can reduce atmospheric temperature or result in climate warming. Streets et al. (2000) suggested that because sulfate aerosols play a vital role in cooling the atmosphere, a reduction in sulfur

dioxide emissions in the future would result in increased global warming. Furthermore, aerosol sulfate has been identified as an important contributor to sunlight scattering (Lelieveld and Heintzenberg, 1992; Kim et al., 2001). At the top of the atmosphere above East Asia, SO_4^{2-} radiative forcing is −2 to −10 W m^{-2} over land and −5 to −15 W m^{-2} over ocean (Gao et al., 2014). Niemeier et al. (2011) revealed that an increase in the SO_2 emission rate does not lead to a similar increase in radiative forcing because, as the size of the aerosols increases, their lifetime decreases. It is thus possible that the sulfur-containing particles transported by an ascending geogas flow have an effect on the climate and should, therefore, be evaluated.

Sulfate particles can be transported into the lungs leading to respiratory illnesses (World Bank Group, 1999; Soleimani et al., 2007). In particular, the sulfur-containing particles contain high levels of toxic Pb, Hg, Cu, and As. In nature, sulfur usually combines with Pb, Hg, Cu, As, Ni, Cd, and Sb, which are toxic to organisms, to form sulfide deposits. The sulfur-containing particles originating from sulfide deposits commonly contain toxic elements. This phenomenon has been confirmed by EDX analysis of particles. The particle sizes carried by the ascending gas flow are usually less than 500 nm. The size is only one-fifth of the upper size limit of PM2.5. Geogas particles have high migration ability and undergo long-distance migration. They can remain in the atmosphere for long periods and in can get into bronchioles and alveoli, affecting the ventilative function of lung. They can also enter the blood. The possible relationship between the occurrence of sulfur-containing particles transported by an ascending geogas flow and endemic diseases in the vicinity of sulfur-containing

deposits should be investigated.

It is probable that sulfur-containing particles transported by the ascending geogas flows in the soil affect the soil system; for example, sulfur-containing particles can affect both soil biota and enzymatic activities, resulting in changes in the soil structure, nutrient cycling, and organic matter decomposition and retention. Sulfur-containing particles may directly catalyze organic matter decomposition. Furthermore, the potential use of such particles as fertilizers for rice plants needs to be investigated.

Acknowledgments

Financial support from the National Natural Science Foundation of China (Grant Nos. 41030425, 41072263, 40773037, and 40673044) and the National High-Tech Research and Development Program of China (863 Program; Grant No. 2008AA06Z101) are gratefully acknowledged.

References

Andres, R. J., Rose, W. I., Stoiber, R. E., Williams, S. N., Matías, O., and Morales, R.: A summary of sulfur dioxide emission rate measurements from Guatemalan volcanoes, B. Volcanol., 55, 379–388, 1993.

Bao, H. M., Yu, S., and Tong, D. Q.: Massive volcanic SO_2 oxidation and sulphate aerosol deposition in Cenozoic North America, Nature, 465, 909–912, 2010.

Berresheim H.: Biogenic sulfur emissions from the Subantarctic and Antarctic Oceans, J. Geophys. Res.. 92, 13245–13262, 1987.

Bhugwant, C., Siéja, B., Bessafi, M., Staudacher, T., and Ecormier, J.: Atmospheric sulfur dioxide measurements during the 2005 and 2007 eruptions of the Piton de

La Fournaise volcano: Implications for human health and environmental changes, J. Volcanol. Geoth. Res., 184, 208–224, 2009.

Cao, J. J.: Migration mechanisms of gold nanoparticles explored in geogas of the Hetai ore district, southern China, Geochem. J., 45, e9–e13, 2011.

Cao, J. J., Hu, R. Z., Liang, Z. R., and Peng, Z. L.: TEM observation of geogas-carried particles from the Changkeng concealed gold deposit, Guangdong Province, South China, J. Geochem. Explor. 101, 247–253, 2009.

Cao, J. J., Hu, X. Y., Jiang, Z. T., Li, H. W., and Zou, X. Z.: Simulation of adsorption of gold nanoparticles carried by gas ascending from the Earth's interior in alluvial cover of the middle-lower reaches of the Yangtze River, Geofluids, 10, 438–446, 2010a.

Cao, J. J., Liu, C., Xiong, Z. H., and Qin, T. R.: 2010b, Particles carried by ascending gas flow at the Tongchanghe copper mine, Guizhou Province, China, Science China Earth Sciences, 53, 1647–1654, 2010b.

Cao, J. J., Liu, C., Zhang, P,, Li, Y. P., and Xiong, Z. H.: The characteristic of geogas particles from Daheishan basalt copper deposit in the Huize county of Yunnan, Mital Mine, 113–115, 2011 (in Chinese with English abstract).

Chenet, A. L., Fluteau, F., and Courtillot, V.: Modelling massive sulfate aerosol pollution, following the large 1783 Laki basaltic eruption, Earth Planet. Sc. Lett. 236, 721–731, 2005.

Çiftçi, E., Kolayli, H., and Tokel, S.: Lead-arsenic soil geochemical study as an exploration guide over the Killik volcanogenic massive sulfide deposit,

Northeastern Turkey, J. Geochem. Explor., 86, 49–59, 2005.

Du, L. T.: The new implication about oil-gas origin and outgassing of the earth obtained in Russia, Ukraine, Azerbaijan in new century, Lithologic Reservoirs, 21(4), 1–9, 2009 (in Chinese with English abstract).

Etiope, G.: Migrazione e comportamento del ‘‘Geogas’’ in bacini argillosi. Ph.D. Thesis, Dept. Earth Sciences, University of Rome ‘‘La Sapienza’’, Extended abstract in Plinius (1996), 15, 90–94, 1995.

Etiope, G.: Subsoil CO_2 and CH_4, and their advective transfer from faulted grassland to the atmosphere, J. Geophys. Res., 104 (D14), 16889–16894, 1999.

Etiope, G., and Martinelli, G., Migration of carrier and trace gases in the geosphere: an overview, Phys. Earth Planet. In., 129, 185–204, 2002.

Gao Y, Zhao C, Liu XH, Zhang MG, and Leung LR, 2014, WRF-Chem simulations of aerosols and anthropogenic aerosol radiative forcing in East Asia. Atmos. Environ., 92, 250–266.

Gierć, R., and Querol, X.: 2010, Atmospheric particles: solid particulate matter in the atmosphere. Elements, 6, 215–222, 2010.

Graf, H.-F., Langmann, B., and Feichter, J.: The contribution of Earth degassing to the atmospheric sulfur budget, Chem. Geol.. 147, 131–145, 1998.

Han, R. S., Liu, C. Q., Huang, Z. L., Chen, J., Ma, D. Y., Lei, L., and Ma, G. S.: Geological features and origin of the Huize carbonate-hosted Zn–Pb–(Ag) District, Yunnan, South China, Ore Geol. Rev., 31, 360–383, 2007.

Hermansson, H.P., Akerblom, G., Chyssler, J., and Linden, A.: Geogas: A Carrier or a

406 Tracer. SKN Report No. 51. National Board for Spent Nuclear Fuel, Stockolm,
407 1–66, 1991.
408 Holub, R. F., Reimer, G. M., Hopke, P. K., Hovorka, J., Krcmar, B., and Smrz, P. K.:
409 "Geoaerosols": their origin, transport and paradoxical behavior: a challenge to
410 aerosol science, J. Aerosol Sci., 30, S111–S112, 1999.
411 Judd, A. G., Davies, J., Wilson, J., Holmes, R., Baron, G., and Bryden, I.:
412 Contributions to atmospheric methane by natural seepages on the UK continental
413 shelf, Mar. Geol., 137, 165–189, 1997.
414 Kiehl, J. T.: Solving the aerosol puzzle, Science, 283, 1273–1275, 1999.
415 Kim, B. G., Park, S. U., and Han, J. S: Transport of SO_2 and aerosol over the Yellow
416 sea, Atmos. Environ., 35, 727–737, 2001.
417 Kristmannsdottir, H., Sigurgeirsson, M., Armannsson, H., Hjartarson, H., and
418 Olafsson, M., Sulfur gas emissions from geothermal power plants in Iceland,
419 Geothermics, 29, 525–538, 2000.
420 Lelieveld, J., and Heintzenberg, J.: Sulfate cooling effect on climate through in-cloud
421 oxidation of anthropogenic SO_2, Science, 258, 117–120, 1992.
422 Liu, C., Cao, J. J., and Ke, H. L.: Geogas characteristic of Yongshengde copper ores in
423 the Northeastern Yunnan, China, Geology of Chemical Minerals, 33, 201–207,
424 2011(in Chinese with English abstract).
425 Liu, Y., Sun, J. R., and Yang, B.: The effects of black carbon and sulfate aerosols in
426 China regions on East Asia monsoons, Tellus B, 61, 642–656, 2009.

427 Malmqvist, L. and Kristiansson, K.: Experimental evidence for an ascending
428 micro-flow of geogas in the ground, Earth Planet. Sc. Lett., 70, 407–423, 1984.

429 Mörner, N.-A. and Etiope, G.: Carbon degassing from the lithosphere, Global Planet.
430 Change, 33, 185–203, 2002.

431 Niemeier, U., Schmidt, H., and Timmreck, C.: The dependency of geoengineered
432 sulfate aerosol on the emission strategy, Atmos. Sci. Lett. Special Issue:
433 Geoengineering, 12, 189–194, 2011.

434 Pósfai, M., Anderson, J. R., and Buseck, P. R.: Soot and sulfate aerosol particles in the
435 remote marine atmosphere, in: Geological Society of America, 1997 annual
436 meeting, Abstracts with Programs - Geological Society of America, 29, 357,
437 1997.

438 Rose, W. I., Chuan, R. L., Giggenbach, W. F., Kyle, P. R., and Symonds, R. B.: Rates
439 of sulfur dioxide and particle emissions from White Island volcano, New
440 Zealand, and an estimate of the total flux of major gaseous species, B. Volcanol.,
441 48, 181–188, 1986.

442 Ruiz, C., Arribas, A., and Arribas, Jr., A.: Mineralogy and geochemistry of the Masa
443 Valverde blind massive sulphide deposit, Iberian Pyrite Belt (Spain), Ore Geol.
444 Rev., 19, 1–22, 2002.

445 Seino, N., Sasaki, H., Sato, J., and Chiba, M.: High-resolution simulation of volcanic
446 sulfur dioxide dispersion over the Miyake Island, Atmos. Environ., 38,
447 7073–7081, 2004.

448 Sinninghe Damsté, J. S., Irene, W., Rijpstra, C., de Leeuw, J. W., and Schenck, P. A.:
449 1988, Origin of organic sulfur compounds and sulfur-containing high molecular
450 weight substances in sediments and immature crude oils, Org. Geochem., 13,
451 593–606, 1988.
452 Soleimani, M., Bassi, A., and Margaritis A.: Biodesulfurization of refractory organic
453 sulfur compounds in fossil fuels, Biotechnol. Adv., 25, 570–596, 2007.
454 Streets, D. G., Tsai, N. Y., Akimoto, H., and Oka, K.: Sulfur dioxide emissions in Asia
455 in the period 1985–1997, Atmos. Environ., 34, 4413–4424, 2000.
456 Sweeney, D., Kyle, P. R., and Oppenheimer, C.: Sulfur dioxide emissions and
457 degassing behavior of Erebus volcano, Antarctica, J. Volcanol. Geoth. Res., 177,
458 725–733, 2008.
459 Tong, C. H., and Li, J. C.: A new method searching for concealed mineral resources:
460 geogas prospecting based on nuclear analysis and accumulation sampling, J.
461 China Univ. Geosci., 10, 329–332, 1999.
462 Trabue, S., Scoggin, K., Mitloehner, F., Li, H., Burns, R., and Xin, H. W.: Field
463 sampling method for quantifying volatile sulfur compounds from animal feeding
464 operations, Atmos. Environ., 42, 3332–3341, 2008.
465 Wei, X. J., Cao, J. J., Holub, R. F., Hopke, P. K., and Zhao, S, J.: TEM study of
466 geogas-transported nanoparticles from the Fankou Lead-Zinc Deposit,
467 Guangdong Province, South China, J. Geochem. Explor., 128, 124–135, 2013.
468 Williams, K. D., Jones, A., Roberts, D. L., Senior, C. A., and Woodage, M. J.: The
469 response of the climate system to the indirect effects of anthropogenic sulfate

aerosol, Clim. Dynam., 17, 845–856, 2001.

Wong, M. H.: An ecological survey of the effect of sulfur dioxide emitted from an Acid Work Factory, B. Environ. Contam. Tox., 19, 715–723, 1978.

World Bank Group: Pollution prevention and abatement handbook: towards cleaner production, World Bank Group Publishers, Washington DC, 1999, 1998.

Wu, T., Wang, X. M., Li, D. J., and Yi, Z. G.: Emission of volatile organic sulfur compounds (VOSCs) during aerobic decomposition of food wastes, Atmos. Environ., 44, 5065–5071, 2010.

Yang, F. G., and Tong, C. H.: Geogas anomaly and mechanism in Xuanhan gas field, Earth Science-Journal of China University of Geosciences, 2000, 25, 103–106 (in Chinese with English abstract).

Yang, Z., Kanda, K., Tsuruta, H., and Minami, K.: Measurement of biogenic sulfur gases emission from some Chinese and Japanese soils, Atmos. Environ., 30, 2399–2405, 1996.

Yang, Z., Kong, U. L., Zhang, J., Wang, L., and Xia, S.: Emission of biogenic sulfur gases from Chinese rice paddies, Sci. Total Environ., 224, 1–8, 1998.

Yuan, L. L.，Wang, M. Q.，and Hu, J. L.: Research of geochemical gas prospecting in sunit, Coal Technology, 33, 85–87, 2014 (in Chinese with English abstract).

Zreda-Gostynska, G., Kyle, P., and Finnegan, D.: Chlorine, fluorine, and sulfur emissions from Mount Erebus, Antarctica and estimated contributions to the Antarctic atmosphere, Geophys. Res. Lett., 20, 1959–1962, 1993.

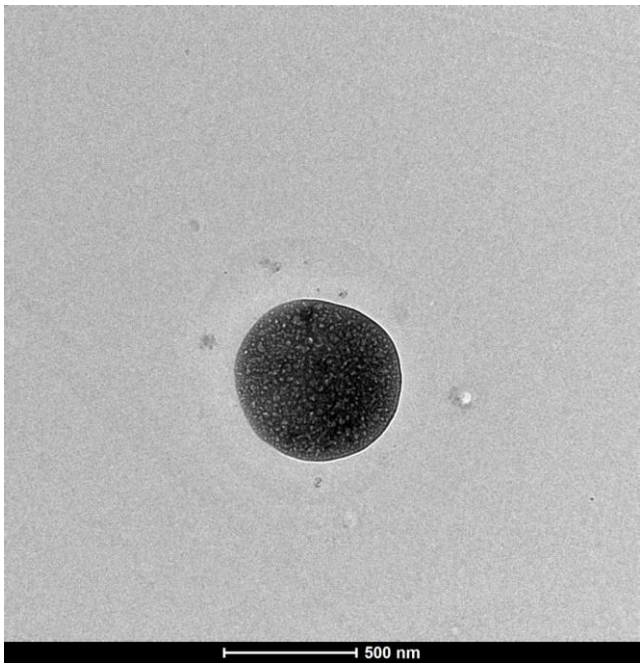

Fig. 1 TEM image of an S-, O-, and Si-containing particle obtained from an ascending gas flow above the soil over the Dongshengmiao deposit.

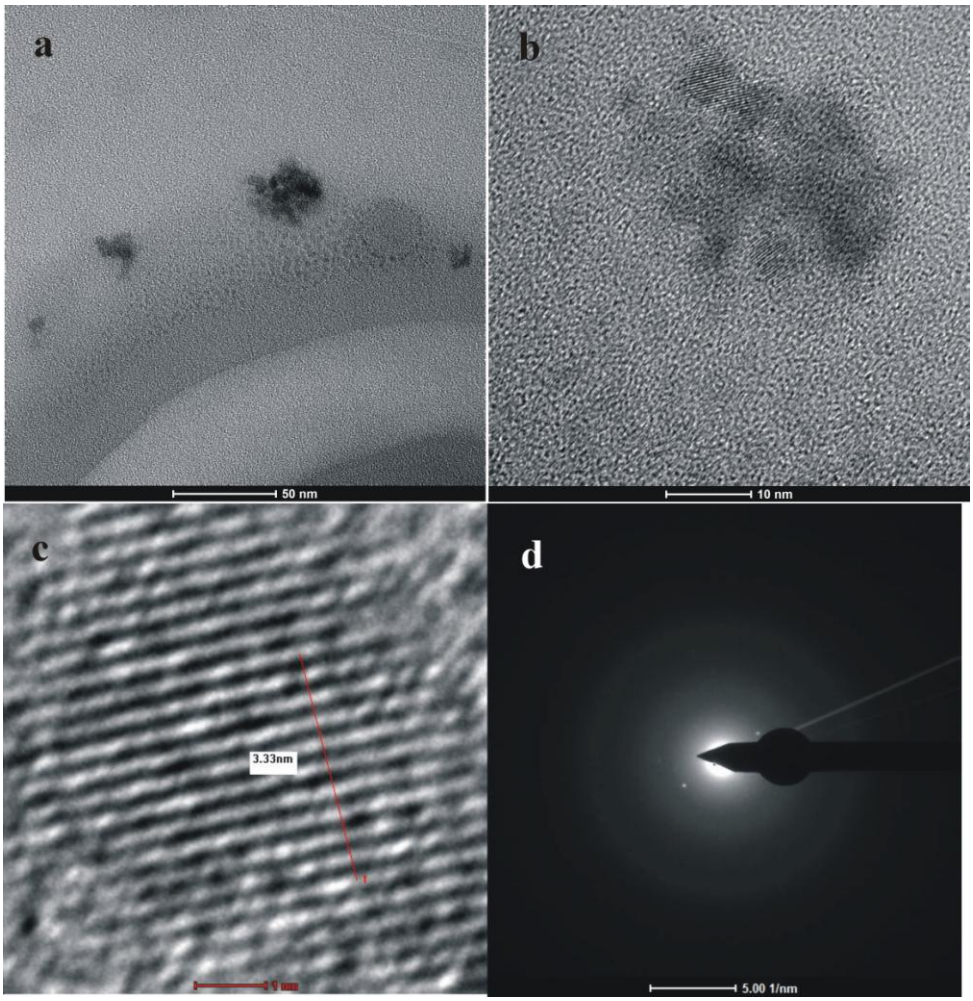

Fig. 2 (a) TEM image, (b, c) high-resolution (HRTEM) images, and (d) selected area electron diffraction (SAED) pattern of an S-, O-, Hg-containing particle aggregation obtained from an ascending gas flow above the soil over the Dongshengmiao deposit.

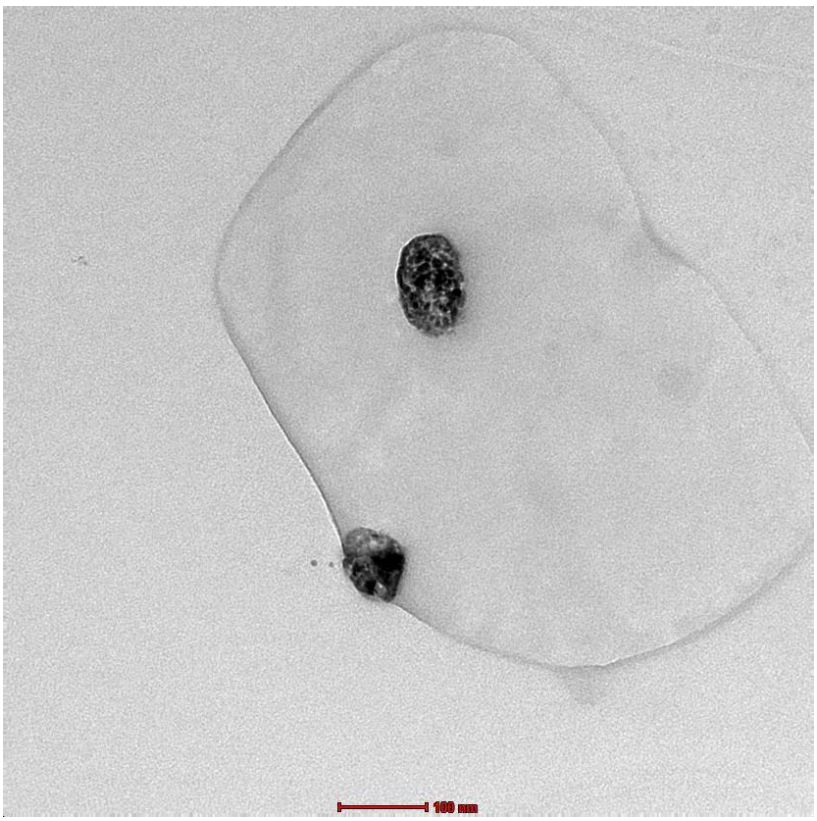

Fig. 3 TEM image of S-, O-, K-, and Pb-containing particle aggregations obtained from an ascending gas flow above the soil over the Dongshengmiao deposit.

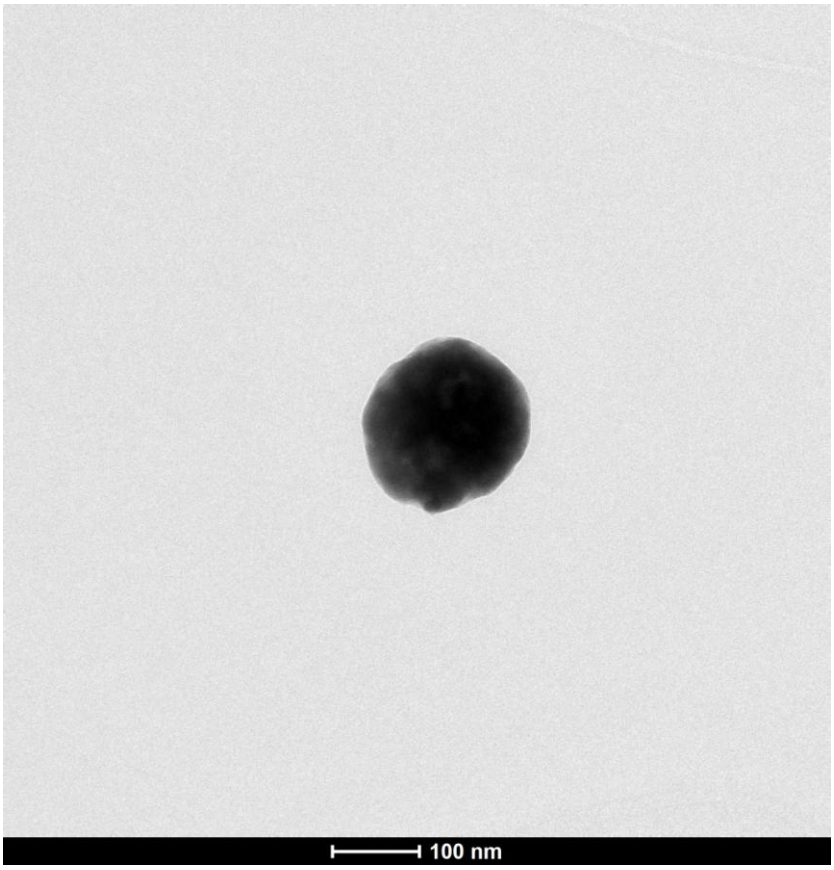

528

529

530 Fig. 4 TEM image of an S-, O-, Na-, Pb-, Zn-, and As-containing particle obtained

531 from an ascending gas flow above the soil over the Dongshengmiao deposit.

532

533

534

535

536

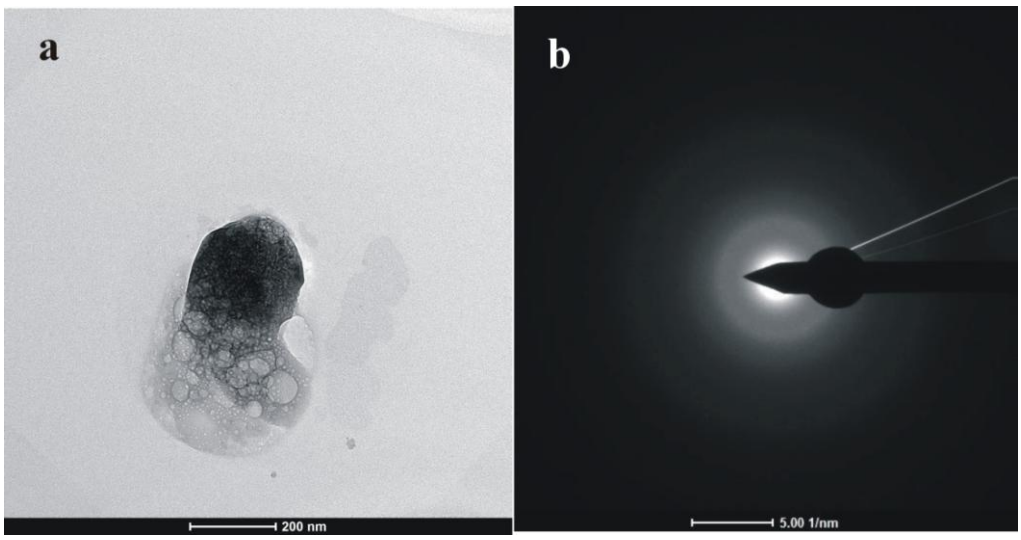

537 Fig. 5 (a) TEM image and (b) SAED pattern of an S-, O-, K-, Na-, and Pb-containing
538 particle obtained from an ascending gas flow above the soil over the Dongshengmiao
539 deposit.

540

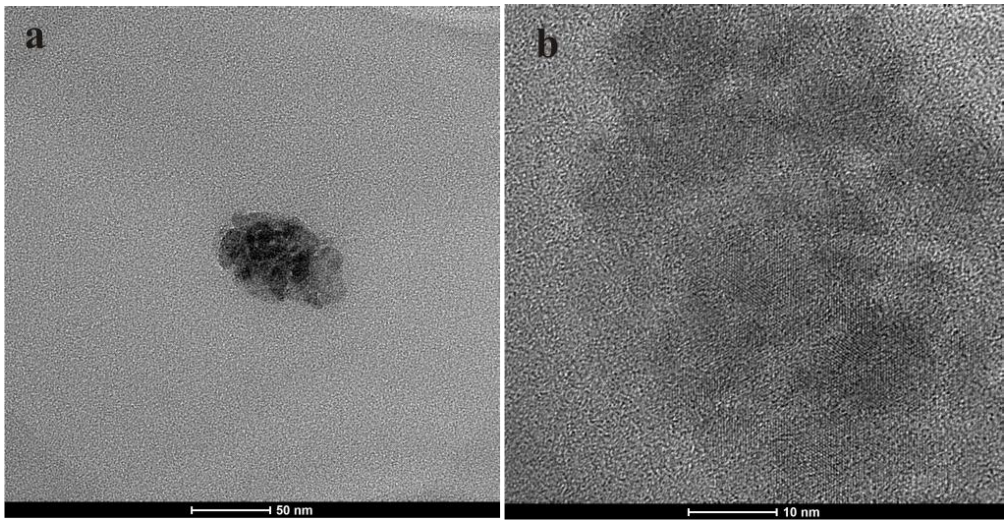

541 Fig. 6 (a) TEM image and (b) HRTEM image of an O-, Si-, S-, and Cu-containing
542 particle aggregation obtained from an ascending gas flow above the soil over the
543 Dongshengmiao deposit.

544

545

546

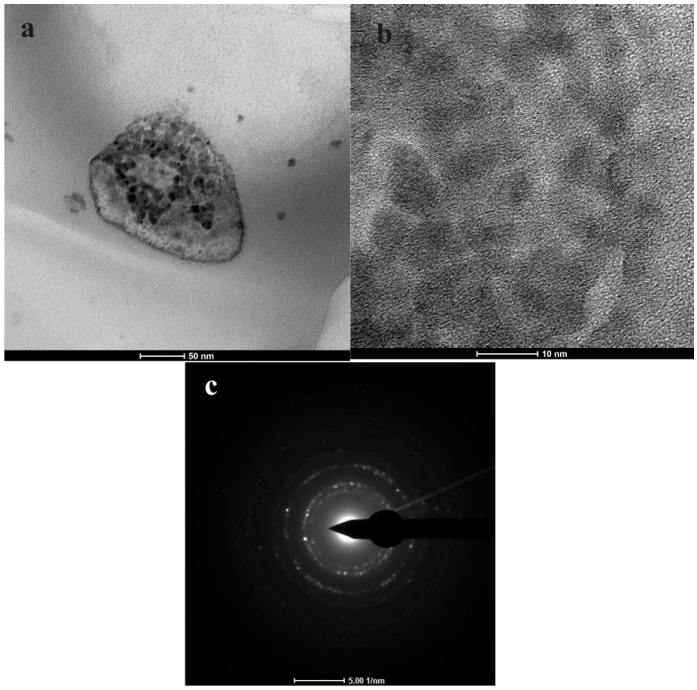

Fig. 7 (a) TEM image, (b)HRTEM image, and (c) SAED pattern of an O-, S-, K-, and Pb-containing particle aggregation obtained from an ascending gas flow above the soil over the Dongshengmiao deposit.

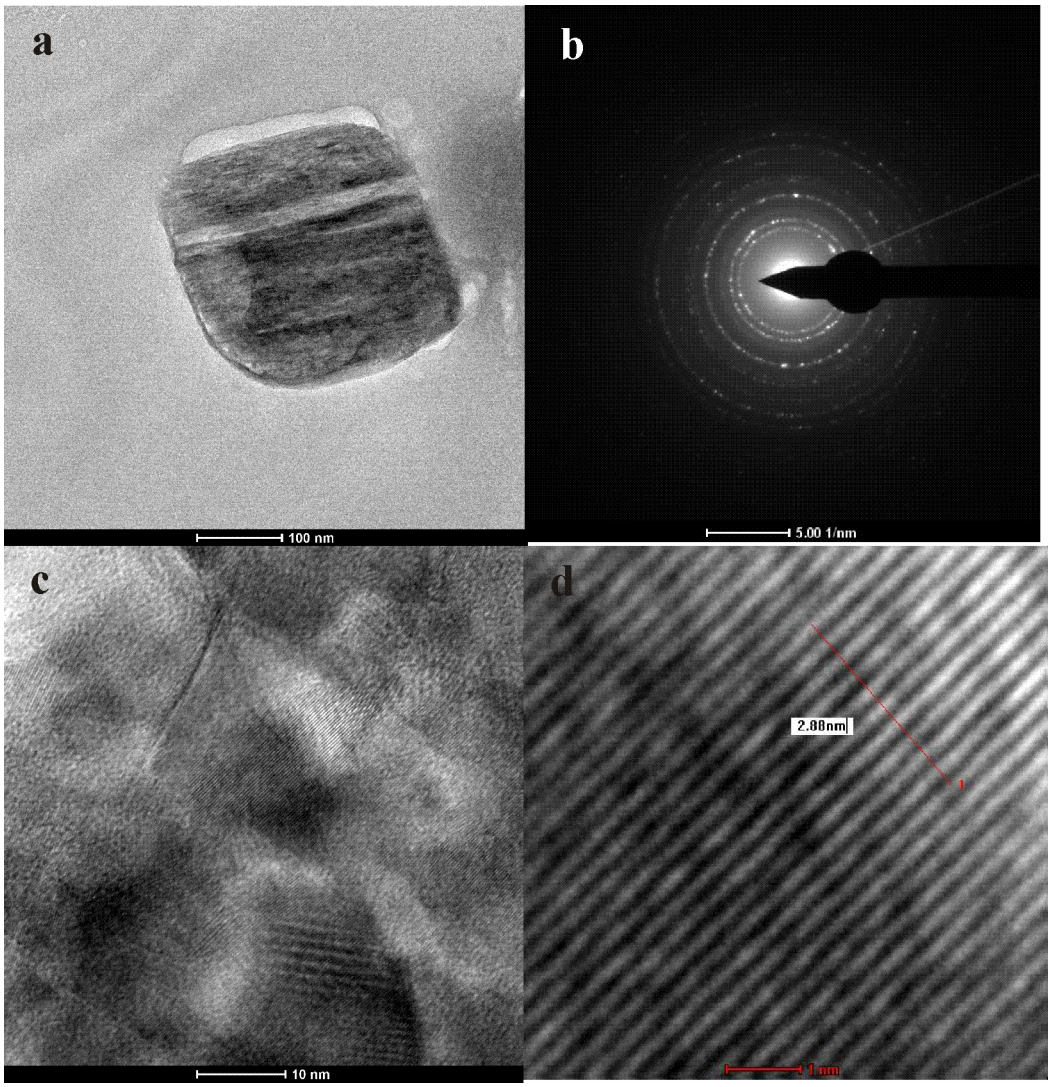

Fig. 8 (a) TEM image, (b) SAED pattern, and (c, d) HRTEM image of an O-, S-, Ca-, and Mg-containing particle obtained from an ascending gas flow in the soil over Dongshengmiao deposit.

581

582

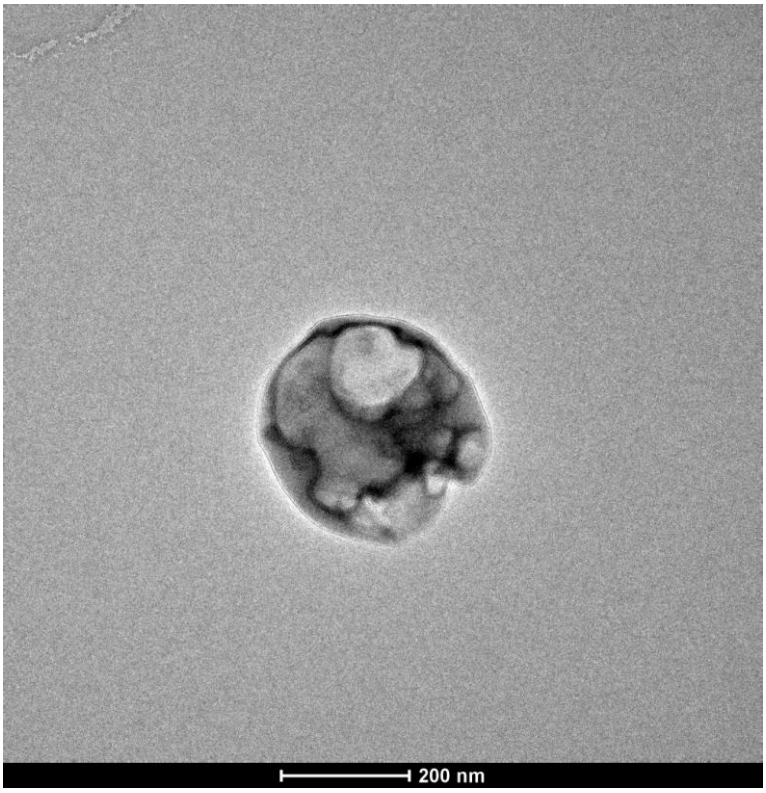

583

584 Fig. 9 TEM image of an O-, S-, and K-containing particle obtained from an ascending

585 gas flow in the soil from the Kafang copper deposit, Yunnan Province.

586

587

588

589

590

591

592

593

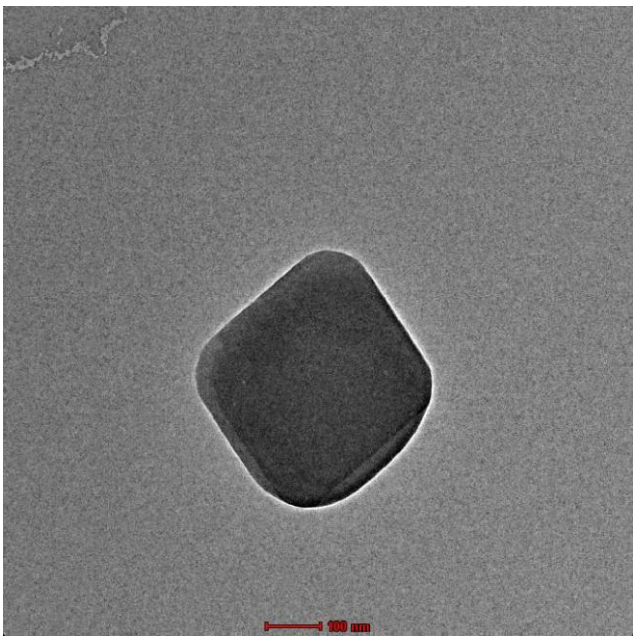

Fig. 10 TEM image of an O-, S-, and Fe-containing particle obtained from an ascending gas flow in the soil from the Yongshengde copper deposit in northeastern Yunnan.

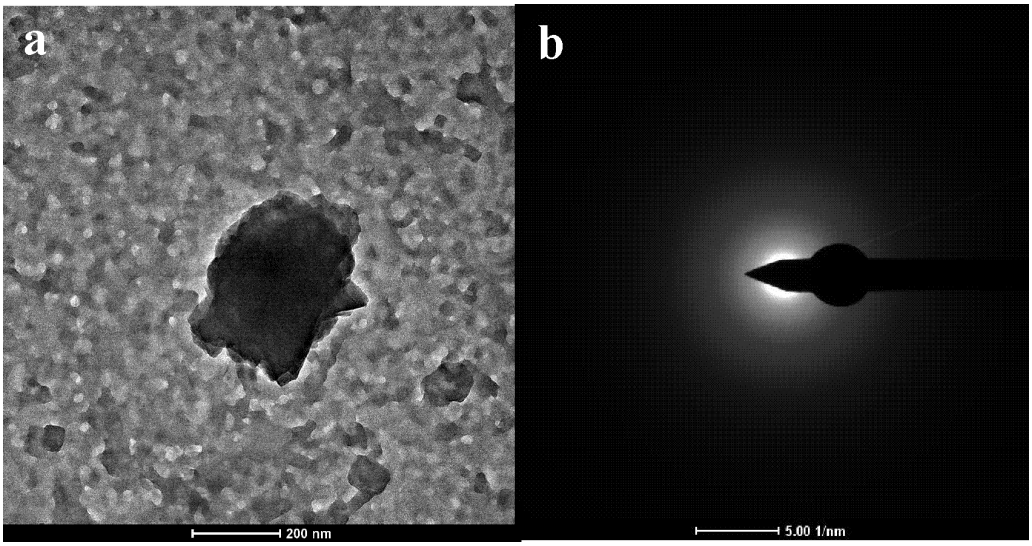

Fig. 11 (a) TEM image and (b) SAED pattern of an O-, S-, and Co-containing particle obtained from an ascending gas flow in the soil from the Qingmingshan Cu–Ni sulfide deposit, Guangxi Province.

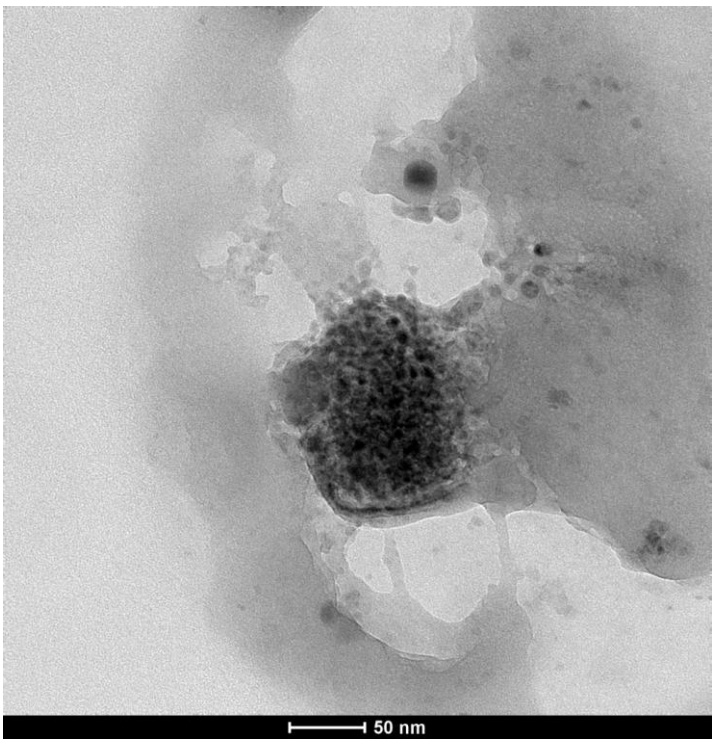

Fig. 12 TEM image of an O-, S-, K-, Pb-, and Na-containing particle sampled using a vacuum pump from the fault gas near a concealed ore body of the Dongshengmiao deposit.

615

616

617

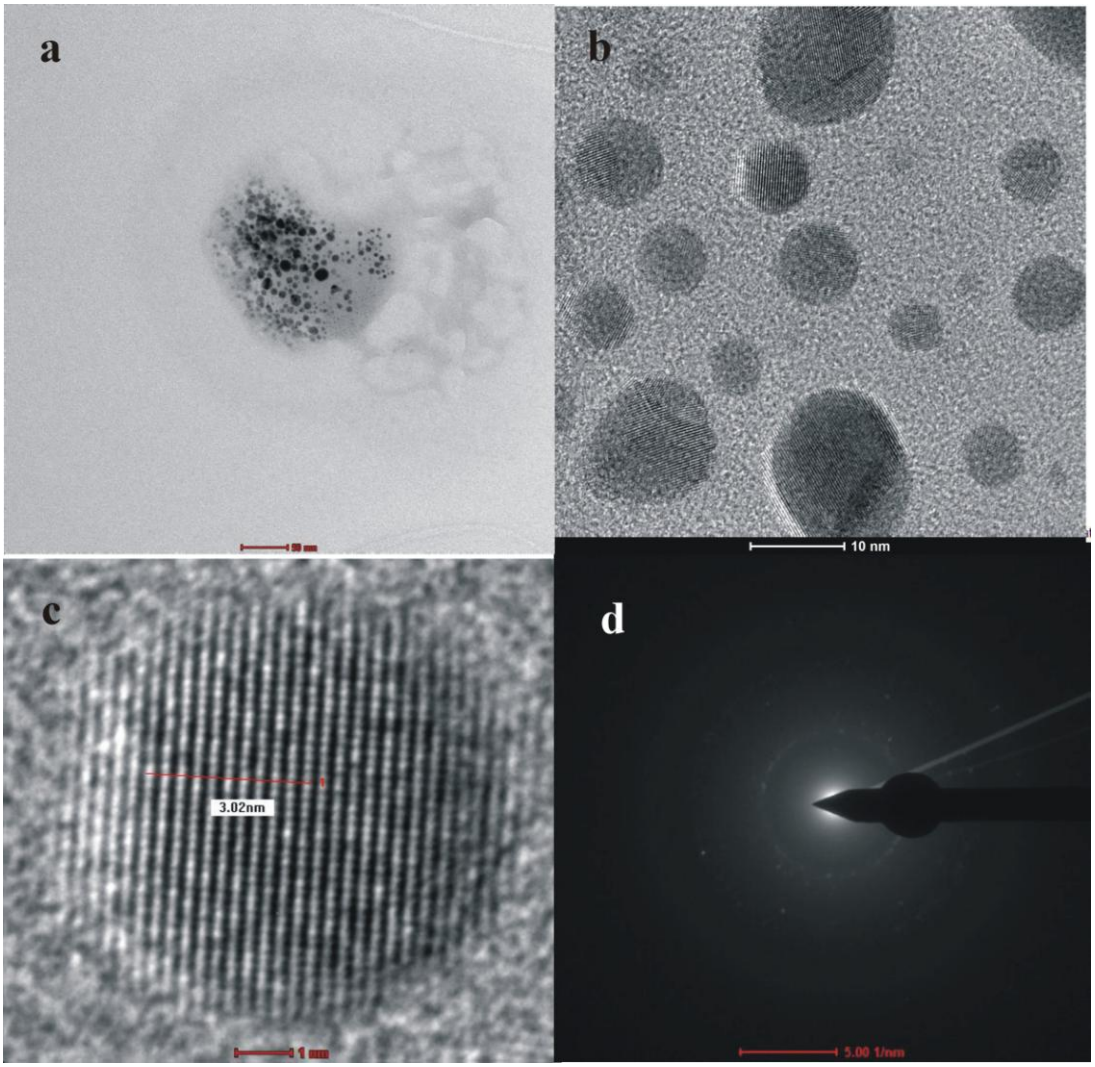

618

619 Fig. 13 (a) TEM image, (b, c) HRTEM images, and (d) SAED pattern of an O-, S-,

620 and K-containing particle aggregation sampled using a PVC pipe in a fault near a

621 concealed ore body of the Dongshengmiao deposit.

622

623

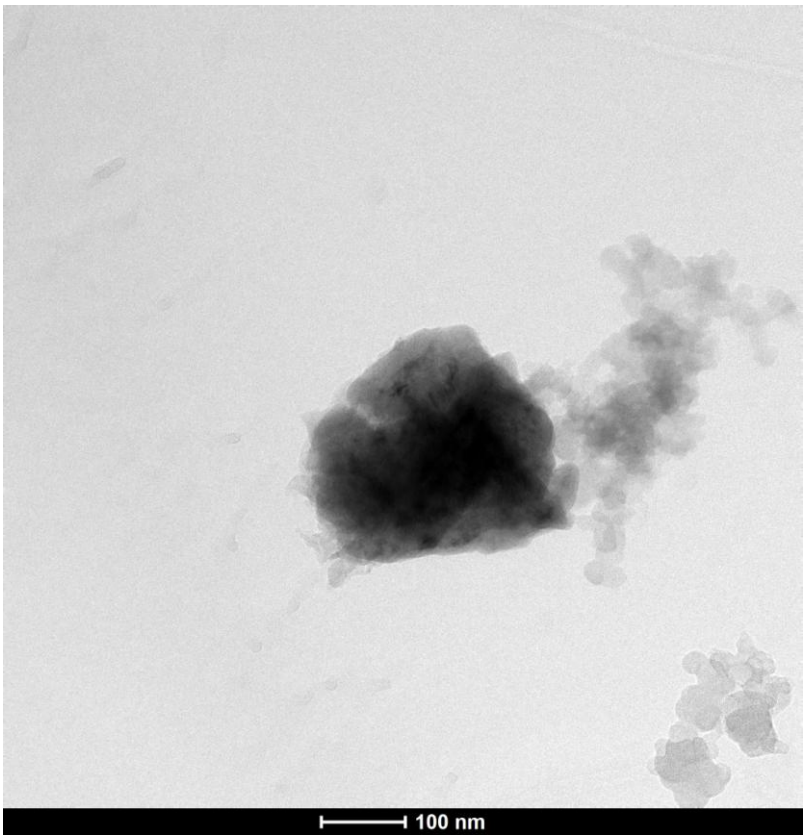

Fig. 14 TEM image of an O-, S-, Fe-, and Mg-containing particle aggregation sampled using a PVC pipe in a fault above a concealed ore body of the Dongshengmiao deposit.

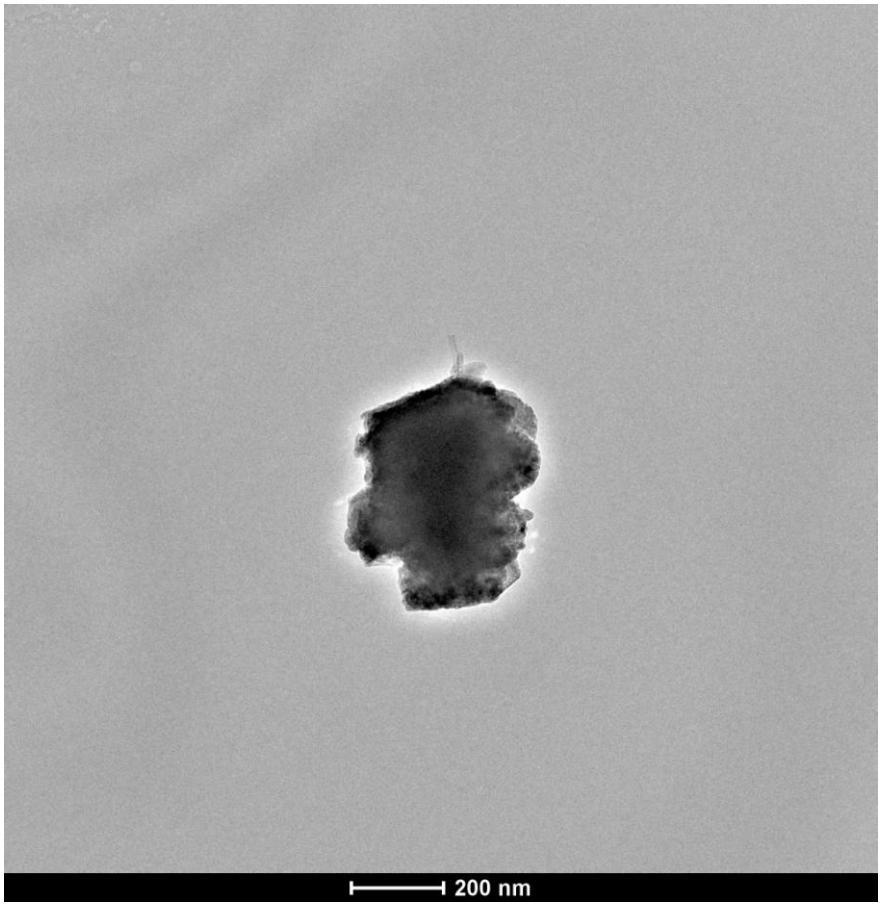

Fig. 15 TEM image of an O-, S-, Ti-, Sr-, and Ba-containing particle from a deep-seated oxidized zone in the Dongshengmiao deposit.

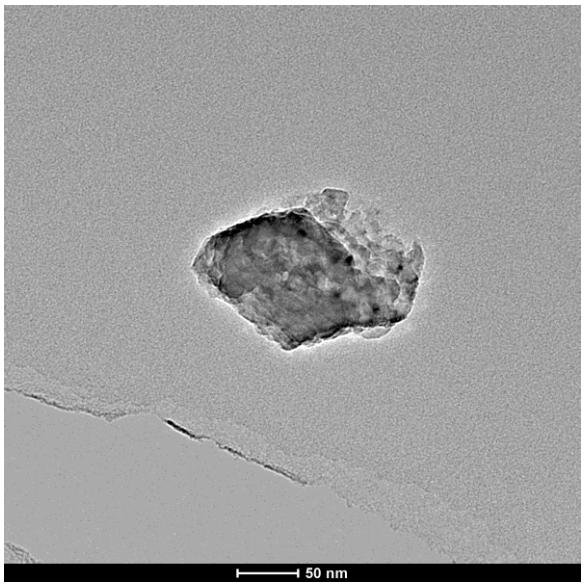

Fig. 16 TEM image of an O-, S-, Fe-, Co-, and Ca-containing particle from a deep-seated fault gouge in the Dongshengmiao deposit.

Table 1 Number of sulfur-containing particles or particle aggregations number from the Dongshengmiao deposit on 100 μm × 100 μm TEM grids

Sulfur-containing particles or particle aggregations carried by ascending gas flow above the soil (that had flown through the soil)				Sulfur-containing particles or particle aggregations carried by ascending gas flow in deep faults			
Sample	Sample box	Grid	Number	Sample	Sample box	Grid	Number
ND13-1	A1	A1-1	3	NDDW03	A2	A2-2	3
ND13-2	A2	A2-1	2	NDDW05	A4	A4-1	1
ND13-3	A3	A3-2	1			A4-2	29
		A3-3	6	NDDW06	A5	A5-2	1
ND13-4	A4	A4-1	1	NDDW07	B1	B1-1	4
		A4-2	2			B1-2	1
ND13-6	A5	A5-1	1	NDDW19	D3	D3-2	1
		A5-2	3			D3-3	2
		A5-3	1	NDDW26	E4	E4-1	1
ND13-8	B2	B2-1	1			E4-3	1
		B2-2	6	NDDW27	E5	E5-1	2
		B2-3	1			E5-3	2
ND13-9	B3	B3-1	1			E5-4	1
		B3-2	1	NDDW36	G4	G4-1	12
		B3-3	1			G4-3	10
ND13-10	B4	B4-1	1			G4-4	1
		B4-3	6	NDDW37	G5	G5-1	1
ND13-11	B5	B5-1	1				

Table 2 EDX results for particles 1–8.

Element	Particle number							
	1	2	3	4	5	6	7	8
Weight O%	18.47	9.46	16.02	9.73	15.75	12.9	5.13	51.88
Atomic O%	31.1	31.78	31.12	39.3	34.16	31.35	22.74	69.78
Weight Si%	3.35		1.49	0.5	1.09	3.08		2.19
Atomic Si%	3.21		1.65	1.15	1.34	4.27		1.67
Weight S%	78.17	31.23	63.1	3.82	10.83	21.61	18.25	19.02
Atomic S%	65.68	52.33	61.16	7.7	11.72	26.2	40.32	12.76
Weight Hg%		59.29						
Atomic Hg%		15.87						
Weight K%			4.88		35.75		7.31	0.99
Atomic K%			3.88		31.73		13.25	0.54
Weight Pb%			14.48	54.2	22.5		69.28	
Atomic Pb%			2.17	16.9	3.76		23.67	
Weight Na%				3.1	9.66			
Atomic Na%				8.73	14.58			
Weight Fe%				0.75	2.14			0.21
Atomic Fe%				0.87	1.33			0.08
Weight Co%				0.98	2.25			
Atomic Co%				1.08	1.32			
Weight Zn%				8.34				
Atomic Zn%				8.24				
Weight As%				18.55				
Atomic As%				16				
Weight Cu%						62.39		
Atomic Cu%						38.16		
Weight Mg%								3.86
AtomicMg%								3.42
Weight Ca%								21.82
Atomic Ca%								11.71

Table 3 EDX results for particles 9–16.

Element	Particle number							
	9	10	11	12	13	14	15	16
Weight O%	26.54	56.25	53.66	25.39	67.03	17.21	29.21	40.8
Atomic O%	42.51	73.54	70.2	37.32	80.72	35.83	64.85	62.97
Weight Si%	0.52			0.66	1	0.7		1.5
Atomic Si%	0.47			0.55	0.68	0.83		1.32
Weight S%	63.99	31.3	42.81	23.8	28.01	24.59	10.88	15.03
Atomic S%	51.15	20.42	27.95	17.45	16.83	25.53	12.05	11.58
Weight K%	8.93	0.78		2.01	2.59			
Atomic K%	5.85	0.42		1.21	1.27			
Weight Pb%				4.25				
Atomic Pb%				0.48				
Weight Na%			1.04	40.92		1.35		
Atomic Na%			0.95	41.84		1.96		
Weight Fe%		9.94	0.44	1.11	1.35	51.16	1.27	5.2
Atomic Fe%		3.72	0.16	0.46	0.46	30.5	0.81	2.3
Weight Co%			2.03					6.36
Atomic Co%			0.72					2.66
Weight Zn%				1.82				
Atomic Zn%				0.65				
Weight Mg%						2.74		
Atomic Mg%						3.75		
Weight Ca%						0.28	0.5	31.08
Atomic Ca%						0.23	0.44	19.15
Weight F%		1.71						
Atomic F%		1.88						
Weight Al%						0.25		
Atomic Al%						0.3		
Weight Mn%						1.68		
Atomic Mn%						1.02		
Weight Ti%							10.94	
Atomic Ti%							8.11	
Weight Sr%							10.32	
Atomic Sr%							4.18	
Weight Ba%							36.86	
Atomic Ba%							9.53	

Table 4 Plasma spectrum S results for liquid collectors along the 1st section (μg/mL)

Number	S	Number	S	Number	S	Number	S
K1-1	0.22	K1-9	0.08	K1-17	0.12	K1-25	0.43
K1-2	0.20	K1-10	0.18	K1-18	0.13	K1-26	0.33
K1-3	0.13	K1-11	0.15	K1-19	0.26	K1-27	0.83
K1-4	0.12	K1-12	0.12	K1-20	0.27	K1-28	0.15
K1-5	0.12	K1-13	0.75	K1-21	0.68	K1-29	0.48
K1-6	0.12	K1-14	0.13	K1-22	0.37	K1-30	0.09
K1-7	0.35	K1-15	0.14	K1-23	0.91	K1-31	0.09
K1-8	0.13	K1-16	0.20	K1-24	0.11		

Table 5 Plasma spectrum S results for liquid collectors along the 2nd section (μg/mL)

Number	S	Number	S	Number	S	Numer	S
K2-1	1.74	K2-20	3.81	K2-39	0.6	K2-59	0.31
K2-2	1.21	K2-21	1.52	K2-40	0.9	K2-60	0.58
K2-3	1.46	K2-22	4.44	K2-41	1.08	K2-61	0.42
K2-4	0.27	K2-23	0.72	K2-42	0.26	K2-62	0.59
K2-5	1.68	K2-24	1.07	K2-43	2.03	K2-63	3.86
K2-6	0.97	K2-25	0.57	K2-44	1.05	K2-64	0.51
K2-7	0.31	K2-26	0.43	K2-45	0.48	K2-65	0.57
K2-8	1.35	K2-27	0.61	K2-46	2.46	K2-66	0.2
K2-9	0.93	K2-28	0.11	K2-47	0.45	K2-67	0.2
K2-10	1.51	K2-29	0.39	K2-48	0.8	K2-68	0.49
K2-11	0.27	K2-30	1.39	K2-49	0.28	K2-69	0.29
K2-12	0.52	K2-31	0.88	K2-50	0.24	K2-70	0.87
K2-13	2.55	K2-32	0.6	K2-51	4.73	K2-71	0.65
K2-14	0.48	K2-33	4.63	K2-52	0.29	K2-72	0.3
K2-15	1.97	K2-34	1.84	K2-53	6.85	K2-73	8.28
K2-16	1.21	K2-35	4.1	K2-54	0.57	K2-74	0.48
K2-17	2.73	K2-36	1.92	K2-55	0.69	K2-75	1.84
K2-18	1.27	K2-37	1.18	K2-56	5.85	K2-76	
K2-19	0.22	K2-38	0.38	K2-57	0.61	K2-77	

Table 6 Plasma spectrum S results for liquid collectors along the 3rd section (μg/mL)

Number	S	Number	S	Number	S	Number	S
K3-1	34.90	K3-6	19.43	K3-11	4.08	K3-16	76.28
K3-2	2.35	K3-7	1.00	K3-12	16.88	K3-17	77.21
K3-3	4.89	K3-8	1.38	K3-13	74.51	K3-18	79.81
K3-4	0.52	K3-9	1.43	K3-14	51.57	K3-19	81.52
K3-5	2.65	K3-10	0.10	K3-15	49.66	K3-20	76.07